EUROPEAN JOURNAL OF PURE AND APPLIED MATHEMATICS
2026, Vol. 19, Issue 1, Article Number 7469
ISSN 1307-5543 – ejpam.com
Published by New York Business Global

Refined LS-Based Generalized Thermoelasticity of a 2D Half-Space Problem with Time-Harmonic Sources

Zahra S. Hafed[1], Ashraf M. Zenkour[1,2,*]

[1] *Department of Mathematics, Faculty of Science, King Khalid University, Abha 21589, Saudi Arabia*
[2] *Department of Mathematics, Faculty of Science, King Abdulaziz University, P.O. Box 80203, Jeddah 21589, Saudi Arabia*
[3] *Department of Mathematics, Faculty of Science, Kafrelsheikh University, Kafrelsheikh 33516, Egypt*

Abstract. The present study develops a generalised version of the exponential Lord-Shulman thermoelasticity theory that takes into account the combined effects of body forces and time-harmonic thermal sources. The appropriate governing equations are generated and analytically solved by means of the harmonic wave technique, assuming that the medium under discussion is traction-free. Displacements, dilatation, temperature distribution, and stress components are among the non-dimensional findings for field variables. Comprehensive numerical evaluations are used to support the explicit analytical formulas developed for these variables. Examining how the operator expansion order and temporal evolution affect the physical fields' behaviour is assumed particular attention. The significance of higher-order modelling in capturing complex dynamic thermoelastic responses is highlighted by graphical representations that unequivocally show that the operator expansion order plays a crucial role in influencing all thermoelastic parameters.

2020 Mathematics Subject Classifications: 74B05, 74A15, 74H10

Key Words and Phrases: Half-space, LS theory, operator expansion order, time-harmonic thermal sources, body forces

1. Introduction

When applying the Lord–Shulman (LS) generalised thermoelastic theory to a half-space, taking body forces into account presents a number of difficulties [1]. The analytical solution of governing equations is made more difficult by the increasing complexity of the interaction between mechanical and thermal fields. Body forces, such as centrifugal and gravitational forces, break symmetry and frequently call for numerical techniques rather than closed-form solutions. Predicting energy dissipation under mechanical and

*Corresponding author.
DOI: https://doi.org/10.29020/nybg.ejpam.v19i1.7469

Email addresses: zenkour@kau.edu.sa, zenkour@sci.kfs.edu.eg (A.M. Zenkour)

thermal loads is made more tough by the thermal relaxation time in LS theory. Boundary conditions must carefully address both mechanical and thermal effects, especially when body forces influence stress and heat flux distributions. Several studies employed LS theory to analyze thermoelastic problems. Sherief and Anwar [2] studied an infinite annular cylinder with traction-free boundaries under thermal loading using LS theory. Laplace transforms and Fourier series inversion were applied, with results compared to coupled thermoelastic models.

In recent decades, generalized thermoelasticity has evolved through a wide spectrum of modern mathematical modeling approaches that extend the classical Lord–Shulman framework to include temperature-dependent properties, multiphysics couplings, microstructure effects, fractional-order formulations, nonlocal theories, and memory-dependent derivatives [3–12]. Othman [3] derived generalized thermoelastic equations using LS theory, accounting for temperature-dependent elasticity in an isotropic medium. Solutions for temperature, displacement, and stress were obtained via normal mode analysis. Othman [4] modeled rotating thermo-viscoelastic half-spaces under thermal shock with one relaxation time. Exact solutions for field variables were derived using normal mode analysis under two boundary conditions. Kumar and Rani [5] analyzed a thermoelastic medium with voids under mechanical and thermal loads. Numerical solutions for field quantities and volume fraction were designed and visualized. For a half-space with constant material properties, Youssef [6] created a unified controlling framework for thermoelasticity that included both classical and generalised theories. El-Maghraby [7] examined the distributions of temperature and stress in a 2D generalised thermoelastic medium exposed to body forces and thermal shock. Abbas et al. [8] used LS theory and finite element methods to examine plane wave propagation in a fiber-reinforced anisotropic thermoelastic half-space under a magnetic field. Sherief et al. [9] explained a 1D problem for a viscoelastic medium and developed equations for generalised thermoviscoelasticity, demonstrating uniqueness and reciprocity theorems. Using Laplace transforms, Sherief and Abd El-Latief [10] utilized fractional-order thermoelasticity to a 1D thermal shock problem in a medium and quantitatively compared the results with coupled and generalised theories. Kiani and Eslami [11] showed a nonlinear thermoelastic study of an isotropic layer using LS theory, retaining the energy equation's nonlinear form without linearization. Rani [12] examined 2D deformation in a generalized thermoelastic medium with voids and microtemperatures under mechanical loading, comparing LS and Green and Lindsay (GL) theories via normal-mode analysis.

Higher-order wave formulations that capture dispersion, attenuation, and relaxation-induced wave phenomena in generalised thermoelastic materials have advanced significantly in tandem with the aforementioned discoveries [13–21]. Singh et al. [13] derived governing equations for isotropic generalized thermoelastic media subjected to hydrostatic initial stress using LS theory. Analytical solutions yielded dimensional wave velocities in the x-y plane. Othman and Singh [14] modeled a rotating micropolar thermoelastic medium exposed to an instantaneous thermal point source on its free surface. Kaushal et al. [15] studied time-harmonic deformation in a two-temperature (2T) generalized thermoelastic half-space using Hankel transforms in the frequency domain. Singh [16]

analyzed Rayleigh surface waves in a 2T thermoelastic medium using LS theory, solving governing equations for wave solutions. Othman and Song [17] studied generalized micropolar magneto-thermoelasticity in a thermally conducting half-space under an axial magnetic field. Singh and Singh [18] analyzed rotational effects on plane waves in a thermo-piezoelectric half-space, incorporating Coriolis and centrifugal forces, and derived solutions for three quasi-plane waves. Sherief et al. [19] solved axi-symmetric 2D viscoelastic problems using Laplace-Hankel transforms and asymptotic expansions to examine wave propagation, with graphical results for temperature, displacement, and stress. Lotfy et al. [20] solved a generalized thermo-microstretch problem for an infinite space with a mode-I crack, subject to prescribed thermal and mechanical loads on the crack surfaces. Tiwari [21] explored variable thermal/electrical conductivity effects in a magnetized half-space under thermal shock using LS theory.

Another active line of research focuses on internal heat-generation mechanisms, including variable thermal conductivity, distributed or moving heat sources, and thermomechanical diffusion effects, which play a central role in transient heating processes [22–29]. Tianhu et al. [22] investigated electromagneto-thermoelastic waves in a semi-infinite conductor under thermal shock and axial magnetic fields using LS generalized thermoelasticity. Youssef and El-Bary [23] developed a 1D generalized thermoelastic theory with variable thermal conductivity for a layered thin plate. Applying Laplace transforms and a direct solution method, they analyzed a thermally shocked, traction-free sandwich structure. Ram et al. [24] provided a general solution for generalized thermodiffusion in elastic solids via Fourier transforms. They demonstrated the approach with concentrated and distributed harmonic sources in the frequency domain. El-Maghraby and Abdel-Halim [25] examined a 2D transient problem for an infinite thermoelastic half-space with axisymmetric temperature distribution and heat sources, using LS theory. Laplace and Hankel transforms were applied for the traction-free boundary. El-Maghraby [26] analyzed a 2D generalized thermoelastic medium exposed to body force and thermal shock, with internal heat sources. Laplace and exponential Fourier transforms were used under the LS theory. Goswami and Sarkar [27] investigated time-harmonic plane waves in an infinite thermoelastic medium using LS theory. Hafed and Zenkour [28] formulated a thermodynamically consistent fractional thermoelasticity model to study the thermal shock response of anisotropic circular hollow cylinders. In a related work [29], they examined the effects of the Lord–Shulman generalized heat conduction theory on an isotropic thermoelastic medium subjected to thermal shock and an applied normal load at its upper boundary.

Complementing these advances are contributions employing advanced numerical and operator-based techniques, such as state-space formulations, high-dimensional coupled solvers, refined multi-phase-lag models, and fractional-order algorithms, that enable accurate simulation of complex thermoelastic fields [30–39]. Youssef and Al-Lehaibi [30] studied a medium with constant elastic parameters using 2T generalized thermoelasticity. Applying Laplace transforms and state-space techniques, they solved for thermal shock and traction-free boundary conditions. Ezzat and Youssef [31] developed a 3D generalized thermoelastic model for a half-space exposed to thermal shock. Laplace and double Fourier transforms solved the coupled equations for a traction-free surface. Tripathi et

al. [32] established a 2D generalized thermoelastic-diffusion model for a half-space with permeating substances using LS theory. Youssef and Al-Lehaibi [33] developed a 3D generalized thermoelastic theory for a half-space under a moving rectangular heat source and a traction-free surface, solved via Laplace and double Fourier transforms. Guo et al. [34] studied thermo-hydro-mechanical interactions in a saturated poroelastic half-space under surface mechanical or thermal loads. Said [35] analyzed wave propagation in a rotating nonlocal generalized thermoelastic medium with a moving internal heat source. Alshaikh [36] modeled generalized thermoelasticity in a porous medium using LS for a 2D isotropic homogeneous fracture field. Sarkar and Singh [37] extended the LS theory by integrating a strain-rate term with a relaxation parameter through extended thermodynamics. Zenkour and Aljadani [38] solved a nonlocal magneto-thermoelastic problem for a thick plate under harmonic heating and magnetic fields using LS theories and Eringen's nonlocal model. Saleh [39] analyzed 1D thermal shock and body force effects in a half-space using Laplace transforms and short-time asymptotic expansions.

Together, these theoretical and computational developments highlight the ongoing need for refined operator expansion strategies, such as the present approach, to accurately represent relaxation effects and wave-based behavior in contemporary generalized thermoelasticity. In most problems of the thermoelasticity theory, the body forces may be neglected. In the present article, we take into consideration the inclusion of the body forces. Also, we suggest that the medium is exposed to both time-harmonic thermal and body force sources. A generalized exponential Lord–Shulman thermoelasticity theory is developed to get the governing equations for the traction-free medium, that solved using Laplace transforms, with numerical inversion applied to obtain nondimensional solutions. Analytical expressions and numerical results for displacements, dilatation, temperature, and stresses were derived, highlighting the substantial influence of operator expansion order and time on all physical quantities.

2. Basic equations and problem formulation

Let us consider a homogeneous, isotropic, thermoelastic medium of infinite extent. A Cartesian coordinate system (x, y, z) is adopted to define the position of any point within the medium at time t. Let u, v denote the mechanical displacement components, σ_{11}, σ_{22}, σ_{12} - the identically non-vanishing stress components in the plane, θ - the temperature measured from a reference temperature T_0, ρ - the mass density, F_1, F_2 - the body force components, q_1, q_2 - the heat flux components, c_E -the specific heat of the solid at constant volume, $\gamma = (3\lambda + 2\mu)\alpha_t$, λ, μ - Lame's constants and α_t -the thermal expansion coefficient. The linear equations of plane generalized thermoelasticity for a transversely isotropic material within the theory of extended thermodynamics read:

Equations of motion

$$\begin{aligned}\frac{\partial \sigma_{11}}{\partial x}+\frac{\partial \sigma_{12}}{\partial y}+F_1&=\rho\frac{\partial^2 u}{\partial t^2},\\ \frac{\partial \sigma_{12}}{\partial x}+\frac{\partial \sigma_{22}}{\partial y}+F_2&=\rho\frac{\partial^2 v}{\partial t^2}.\end{aligned} \tag{1}$$

Heat equation

$$\frac{\partial q_1}{\partial x}+\frac{\partial q_2}{\partial y}=-\rho c_E\frac{\partial \theta}{\partial t}-T_0\gamma\frac{\partial}{\partial t}\left(\frac{\partial u}{\partial x}+\frac{\partial v}{\partial y}\right). \tag{2}$$

The thermoelastic generalized Hooke's law

$$\begin{aligned}\sigma_{11}&=(\lambda+2\mu)\frac{\partial u}{\partial x}+\lambda\frac{\partial v}{\partial y}-\gamma\theta,\\ \sigma_{22}&=\lambda\frac{\partial u}{\partial x}+(\lambda+2\mu)\frac{\partial v}{\partial y}-\gamma\theta,\\ \sigma_{12}&=\mu\left(\frac{\partial v}{\partial x}+\frac{\partial u}{\partial y}\right).\end{aligned} \tag{3}$$

The heat conduction equation (2), according to Lord and Shulman's thermoelasticity theory in its refined form [1, 38, 40–43], is given by

$$K\nabla^2\theta=\mathcal{D}_0\left[\rho c_E\frac{\partial \theta}{\partial t}+T_0\gamma\frac{\partial}{\partial t}\left(\frac{\partial u}{\partial x}+\frac{\partial v}{\partial y}\right)+\rho Q\right], \tag{4}$$

where K is the thermal conductivity, $\nabla^2=\frac{\partial^2}{\partial x^2}+\frac{\partial^2}{\partial y^2}$, and Q is the internal heat source. The differential operator $\mathcal{D}_0$ is expressed as

$$\mathcal{D}_0=\sum_{n=0}^{N}\frac{\tau^n}{n!}\frac{\partial^n}{\partial t^n}, \tag{5}$$

where N may be denoted by the operator expansion order, and τ is the relaxation time.

In the following, we focus on determining all field variables for various values of N. Special attention is given to the case $N\to\infty$, which is of particular significance and is considered here within the framework of generalized thermoelasticity. If we analyze the operator in Eq. (5) as $N\to\infty$, we get

$$\mathcal{D}_0\to \mathrm{e}^{\tau\partial_t},\quad \partial_t=\frac{\partial}{\partial t}, \tag{6}$$

which corresponds to the exponential time-shift operator, i.e.,

$$\mathrm{e}^{\tau\partial_t}f(r,t)=f(r,t+\tau). \tag{7}$$

Equation (4) may be dealt with the simple LS thermoelasticity theory when $N=1$.

3. Formulation of the problem

The bounding surface of the solid is taken to be traction-free and is subjected to time-harmonic thermal and mechanical sources. All associated field quantities, such as displacement components, temperature change, and stress fields, are functions of the coordinates x, y, and time t only, implying a two-dimensional formulation where no variation occurs along the z-axis.

The heat conduction equation without any heat source is

$$K\nabla^2\theta = \mathcal{D}_1\left(\rho c_E\theta + \gamma T_0 e\right), \tag{8}$$

where

$$e = \frac{\partial u}{\partial x} + \frac{\partial v}{\partial y}, \quad \mathcal{D}_1 = \mathcal{D}_0\frac{\partial}{\partial t} = \sum_{n=0}^{N}\frac{\tau^n}{n!}\frac{\partial^{n+1}}{\partial t^{n+1}}. \tag{9}$$

When $N \to \infty$, $\mathcal{D}_1 = \frac{\partial}{\partial t}\mathrm{e}^{\tau\partial_t}$.

The equation of motion presented by the displacement components is

$$\begin{aligned}
\mu\nabla^2 u + (\lambda+\mu)\frac{\partial e}{\partial x} + F_1 - \gamma\frac{\partial\theta}{\partial x} &= \rho\frac{\partial^2 u}{\partial t^2},\\
\mu\nabla^2 v + (\lambda+\mu)\frac{\partial e}{\partial y} + F_2 - \gamma\frac{\partial\theta}{\partial y} &= \rho\frac{\partial^2 v}{\partial t^2}.
\end{aligned} \tag{10}$$

4. Solution of the problem

4.1. Dimensionless forms

To transform the above equations into dimensionless forms, we define the following nondimensional variables:

$$\begin{aligned}
&\{x', y', u', v'\} = \frac{c_0}{\eta}\{x, y, u, v\}, \quad \{t', \tau'\} = \frac{c_0^2}{\eta}\{t, \tau\}, \quad \theta' = \frac{\gamma}{\rho c_0^2}\theta,\\
&\sigma'_{ij} = \frac{1}{\rho c_0^2}\sigma_{ij}, \quad F_i' = \frac{\eta}{\rho c_0^3}F_i, \quad c_0^2 = \frac{\lambda+2\mu}{\rho}, \quad \eta = \frac{K}{\rho c_E}.
\end{aligned} \tag{11}$$

Then, using Eq. (11), the dimensionless dilatation, stresses, equations of motion, and heat equation become (omitting the prime)

$$e = \frac{\partial u}{\partial x} + \frac{\partial v}{\partial y}, \tag{12}$$

$$\begin{aligned}
\sigma_{11} &= \frac{\partial u}{\partial x} + c_1\frac{\partial v}{\partial y} - \theta,\\
\sigma_{22} &= c_1\frac{\partial u}{\partial x} + \frac{\partial v}{\partial y} - \theta,\\
\sigma_{12} &= c_2\left(\frac{\partial v}{\partial x} + \frac{\partial u}{\partial y}\right),
\end{aligned} \tag{13}$$

$$\begin{aligned}
&\frac{\partial^2 u}{\partial x^2}+c_1\frac{\partial^2 v}{\partial x\partial y}+c_2\frac{\partial}{\partial y}\left(\frac{\partial u}{\partial y}+\frac{\partial v}{\partial x}\right)+F_1-\frac{\partial \theta}{\partial x}=\frac{\partial^2 u}{\partial t^2},\\
&\frac{\partial^2 v}{\partial y^2}+c_1\frac{\partial^2 u}{\partial x\partial y}+c_2\frac{\partial}{\partial x}\left(\frac{\partial u}{\partial y}+\frac{\partial v}{\partial x}\right)+F_2-\frac{\partial \theta}{\partial y}=\frac{\partial^2 v}{\partial t^2},
\end{aligned} \tag{14}$$

$$\left(\frac{\partial^2}{\partial x^2}+\frac{\partial^2}{\partial y^2}\right)\theta=\mathcal{D}_1\left[\theta+\varepsilon\left(\frac{\partial u}{\partial x}+\frac{\partial v}{\partial y}\right)\right], \tag{15}$$

where

$$c_1=\frac{\lambda}{\lambda+2\mu},\quad c_2=\frac{\mu}{\lambda+2\mu},\quad \varepsilon=\frac{\gamma^2 T_0}{\rho^2 c_0^2 c_E}. \tag{16}$$

4.2. Solution due to the Helmholtz decomposition approach

The Helmholtz decomposition technique is a mathematical tool employed to simplify and analyze vector fields by resolving them into irrotational (curl-free) and solenoidal (divergence-free) components. In the framework of thermoelasticity, particularly within generalized theories such as Lord–Shulman, this method proves especially useful for addressing coupled displacement fields that arise from the interaction of mechanical and thermal phenomena. We will apply Helmholtz decomposition to the displacements u and v to simplify the governing equations.

$$u=\frac{\partial \phi}{\partial x}+\frac{\partial \psi}{\partial y},\quad v=\frac{\partial \phi}{\partial y}-\frac{\partial \psi}{\partial x}, \tag{17}$$

where ϕ is the scalar potential (related to dilatational waves), and ψ is the vector potential (related to shear waves). Once again, the harmonic wave solution to the derived system of partial differential equations can be assumed using the method of separation of variables, expressed as

$$\{\phi,\psi,\theta\}(x,y,t)=\{\phi^*,\psi^*,\theta^*\}(x)\mathrm{e}^{\omega t+\imath m y}, \tag{18}$$

where ϕ^* and ψ^* are additional amplitudes of the corresponding functions, ω is a complex frequency, $\imath=\sqrt{-1}$, and m is a real wave number in the y-direction. In addition, the components of the body force are considered as

$$\{F_1,F_2\}(x,y,t)=\left\{\mathrm{e}^{-\Omega_1 x},\mathrm{e}^{-\Omega_2 x}\right\}\mathrm{e}^{\omega t+\imath m y}, \tag{19}$$

in which Ω_1, Ω_2 are constants. The equations of motion become

$$\left(\frac{\mathrm{d}^2}{\mathrm{d}x^2}-2c_3\right)\phi^*-\theta^*=\frac{1}{\Omega_1}\mathrm{e}^{-\Omega_1 x}, \tag{20}$$

$$\left(\frac{\mathrm{d}^2}{\mathrm{d}x^2}-\xi_3^2\right)\psi^*=-\frac{1}{\Omega_2 c_2}\mathrm{e}^{-\Omega_2 x}, \tag{21}$$

$$\left(\frac{\mathrm{d}^2}{\mathrm{d}x^2} - 2c_4\right)\theta^* - \left(2c_5\frac{d^2}{dx^2} - c_6\right)\phi^* = 0, \tag{22}$$

where

$$\begin{aligned} &c_3 = \frac{1}{2}\left(m^2+\omega^2\right), \quad c_4 = \frac{1}{2}\left(m^2+\overline{\mathcal{D}}_1\right), \quad c_5 = \frac{1}{2}\varepsilon\overline{\mathcal{D}}_1, \quad c_6 = \varepsilon m^2\overline{\mathcal{D}}_1, \\ &\xi_3^2 = \frac{c_2m^2+\omega^2}{c_2}, \quad \overline{\mathcal{D}}_1 = \sum_{n=0}^{N}\frac{\tau^n}{n!}\omega^{n+1}. \end{aligned} \tag{23}$$

When $N\to\infty$, $\overline{\mathcal{D}}_1 = \omega\mathrm{e}^{\omega\tau}$.

The solution of Eqs. (20) and (22) are given by

$$\{\theta^*,\phi^*\} = \sum_{i=1}^{2}\{1,\ \beta_i\}\,A_i\mathrm{e}^{-\xi_i x} + \left\{\overline{\Omega}_1,\overline{\Omega}_2\right\}\mathrm{e}^{-\Omega_1 x}, \tag{24}$$

where A_i are the integration parameters, and ξ_i are the following roots:

$$\begin{aligned} &\xi_1^2,\xi_2^2 = c_3+c_4+c_5\mp\xi_0, \\ &\xi_0^2 = c_3^2 - 2c_3\left(c_4-c_5\right) + \left(c_4+c_5\right)^2 - c_6. \end{aligned} \tag{25}$$

The coefficients β_i and $\overline{\Omega}_i$ in Eq. (24) are given by

$$\begin{aligned} &\beta_i = \frac{c_3-c_4-c_5\mp\xi_0}{4c_3c_5-c_6}, \quad \overline{\Omega}_1 = \frac{2\Omega_1^2c_5-c_6}{\Omega}, \quad \overline{\Omega}_2 = \frac{\Omega_1^2-2c_4}{\Omega}, \\ &\Omega = \Omega_1\left[\Omega_1^4 - 2\Omega_1^2\left(c_3+c_4+c_5\right) + 4c_3c_4+c_6\right]. \end{aligned} \tag{26}$$

Also, the solution of Eq. (21) yields

$$\psi^* = A_3\mathrm{e}^{-\xi_3 x} + \Omega_3\mathrm{e}^{-\Omega_2 x}, \tag{27}$$

where A_3 is an additional integration parameter and

$$\Omega_3 = \frac{1}{\Omega_2c_2\left(\xi_3^2-\Omega_2^2\right)}. \tag{28}$$

So, the displacements, dilatation, and stresses of the half-space according to the Helmholtz decomposition method are expressed as

$$u = \left[\sum_{i=1}^{2}\beta_i\xi_iA_i\mathrm{e}^{-\xi_i x} + \imath m\left(A_3\mathrm{e}^{-\xi_3 x} + \Omega_3\mathrm{e}^{-\Omega_2 x}\right) - \Omega_1\overline{\Omega}_2\mathrm{e}^{-\Omega_1 x}\right]\mathrm{e}^{\omega t+\imath my}, \tag{29}$$

$$v = \left[\sum_{i=1}^{2}\imath m\beta_iA_i\mathrm{e}^{-\xi_i x} + \xi_3A_3\mathrm{e}^{-\xi_3 x} + \imath m\overline{\Omega}_2\mathrm{e}^{-\Omega_1 x} + \Omega_2\Omega_3\mathrm{e}^{-\Omega_2 x}\right]\mathrm{e}^{\omega t+\imath my}, \tag{30}$$

$$e = \left[\sum_{i=1}^{2} \left(\xi_i^2 - m^2\right) \beta_i A_i \mathrm{e}^{-\xi_i x} + \overline{\Omega}_2 \left(\Omega_1^2 - m^2\right) \mathrm{e}^{-\Omega_1 x}\right] \mathrm{e}^{\omega t + \imath m y}, \tag{31}$$

$$\begin{Bmatrix} \sigma_{11} \\ \sigma_{22} \\ \sigma_{12} \end{Bmatrix} = \left[\sum_{i=1}^{2} \begin{Bmatrix} \kappa_i \\ \zeta_i \\ \vartheta_i \end{Bmatrix} A_i \mathrm{e}^{-\xi_i x} + \begin{Bmatrix} \kappa_3 \\ \zeta_3 \\ \vartheta_3 \end{Bmatrix} A_3 \mathrm{e}^{-\xi_3 x} + \begin{Bmatrix} \kappa_4 \\ \zeta_4 \\ \vartheta_4 \end{Bmatrix} \mathrm{e}^{-\Omega_1 x} + \begin{Bmatrix} \kappa_5 \\ \zeta_5 \\ \vartheta_5 \end{Bmatrix} \mathrm{e}^{-\Omega_2 x}\right] \mathrm{e}^{\omega t + \imath m y}, \tag{32}$$

where

$$\begin{aligned}
&\kappa_i = \beta_i \left(\xi_i^2 - c_1 m^2\right) - 1, \quad \zeta_i = \beta_i \left(c_1 \xi_i^2 - m^2\right) - 1, \quad \vartheta_i = -2\imath m \beta_i \xi_i c_2, \\
&\kappa_3 = \imath m \left(c_1 - 1\right) \xi_3, \quad \zeta_3 = -\kappa_3, \quad \vartheta_3 = -c_2 \left(\xi_3^2 + m^2\right), \\
&\kappa_4 = \overline{\Omega}_2 \left(\Omega_1^2 - c_1 m^2\right) - \overline{\Omega}_1, \quad \zeta_4 = \overline{\Omega}_2 \left(\Omega_1^2 c_1 - m^2\right) - \overline{\Omega}_1, \quad \vartheta_4 = -2\imath m \Omega_1 \overline{\Omega}_2 c_2, \\
&\kappa_5 = \imath m \Omega_2 \Omega_3 \left(c_1 - 1\right), \quad \zeta_5 = -\kappa_5, \quad \vartheta_5 = -c_2 \Omega_3 \left(\Omega_2^2 + m^2\right).
\end{aligned} \tag{33}$$

The boundary conditions at $x = 0$ are considered as

$$\theta = \theta_0, \quad \sigma_{11} = \sigma_{12} = 0. \tag{34}$$

After applying the above boundary conditions, one can obtain the integration constants in the form:

$$A_j = \frac{\Delta_j}{\Delta}, \quad j = 1, 2, 3, \tag{35}$$

where

$$\begin{aligned}
\Delta &= \vartheta_3 \left(\kappa_1 - \kappa_2\right) + \kappa_3 \left(\vartheta_2 - \vartheta_1\right), \\
\Delta_1 &= \vartheta_3 [\left(\overline{\Omega}_1 - \theta_0\right) \kappa_2 - \kappa_4 - \kappa_5] - \kappa_3 [\left(\overline{\Omega}_1 - \theta_0\right) \vartheta_2 - \vartheta_4 - \vartheta_5], \\
\Delta_2 &= \kappa_3 \left[\left(\overline{\Omega}_1 - \theta_0\right) \vartheta_1 - \vartheta_4 - \vartheta_5\right] - \vartheta_3 \left[\left(\overline{\Omega}_1 - \theta_0\right) \kappa_1 - \kappa_4 - \kappa_5\right], \\
\Delta_3 &= \left(\overline{\Omega}_1 - \theta_0\right) \left(\kappa_1 \vartheta_2 - \kappa_2 \vartheta_1\right) + \left(\kappa_4 + \kappa_5\right) \left(\vartheta_1 - \vartheta_2\right) - \left(\kappa_1 - \kappa_2\right) \left(\vartheta_4 + \vartheta_5\right).
\end{aligned} \tag{36}$$

5. Numerical results and discussions

Figures 1–14 show all variables along the x-direction of the medium using the refined LS thermoelasticity theory. To demonstrate the analytical procedure outlined above, we now consider a numerical example. The considered half-space is composed of silicon, characterized by the following material properties:

$$\begin{aligned}
&\lambda = 7.76 \times 10^{10} \text{ N/m}^2, \quad \mu = 3.86 \times 10^{10} \text{ N/m}^2, \quad \rho = 8954 \text{ kg/m}^3, \quad T_0 = 293 \text{ K}, \\
&c_E = 383.1 \text{ J/(kg K)}, \quad \alpha = 1.78 \times 10^{-5} \text{ N/(m}^2\text{K)}, \quad K = 386 \text{ W/(mK)}.
\end{aligned} \tag{37}$$

The thermoelastic solution for the half-space is finished by the application of the boundary conditions. For simplicity, the numerical outcomes are offered by means of realistic estimates of thermoelastic variables. These results are gained for $t = 0.5$, $\tau = 0.35$, $m = \pi/5$, $\omega = -0.95 - 1.25\,\imath$, $\Omega_1 = \Omega_2 = 10^3$, and $\theta_0 = 10$. This work contains 14 figures that

analyze various aspects of thermoelastic behavior in a half-space under time-harmonic sources, comparing various theories and parameters.

We evaluate the field variables for different N cases with the case $N\to\infty$ addressed in generalized thermoelasticity. Figures 1–7 compare the effect of the values of the operator expansion order N on the temperature distribution (θ), displacement distributions (u and v), dilatation (e), normal stresses (σ_{11} and σ_{22}), and tangential stress (σ_{12}). The case of $N\to\infty$ (the exponential case) is considered in Figures 8–14 to discuss the effect of the time parameter on all field variables.

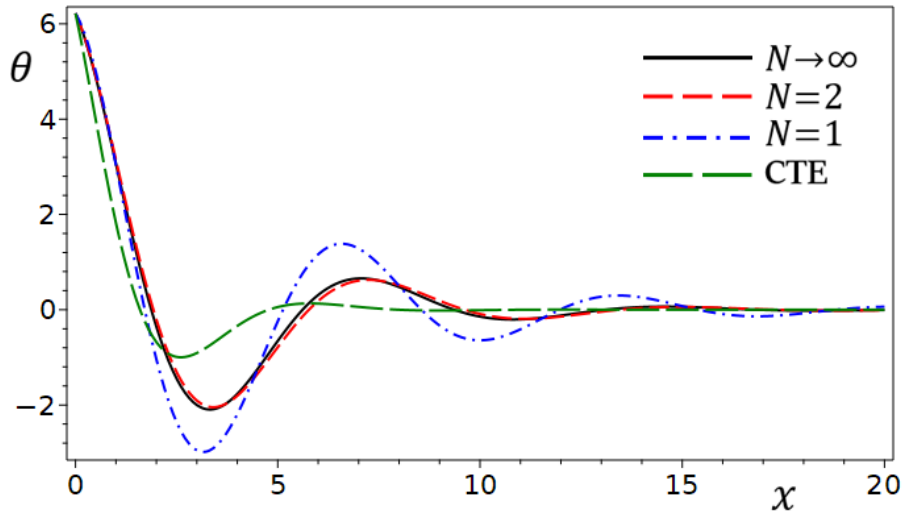

Figure 1: Variation of temperature distribution θ with horizontal distance x for different N using CTE and LS theories.

Figure 1 displays the variation of temperature distribution θ with horizontal distance x using classical thermoelasticity (CTE) theory and Lord–Shulman (LS) thermoelasticity theory for different N. All curves start from the same initial value of θ. The peak temperature is highest at the origin and then decays with increasing x. For $N = 1$ (simple LS theory), the temperature curve shows stronger oscillations with higher amplitude. For $N = 2$, oscillations are reduced, and the curve lies closer to the limiting case. For $N \to \infty$, the oscillations are further suppressed, and the curve smooths out, approaching a stable distribution. The CTE solution exhibits a much smoother decay without pronounced oscillations, reflecting the instantaneous propagation assumption. In contrast, LS theory (with finite N) captures wave-like effects due to thermal relaxation time, leading to oscillatory behavior. As N increases, the LS results tend toward the CTE curve but still retain wave-like features. All LS curves ($N \geq 1$) converge gradually toward zero with diminishing oscillations. The CTE curve also tends to zero but more smoothly, with no oscillations.

Figure 2 displays the variation of displacement distribution u with horizontal distance x using CTE theory and LS thermoelasticity theory for different N. The displacement u starts with a steep negative value at $x = 0$, then rises sharply to a positive peak. The max-

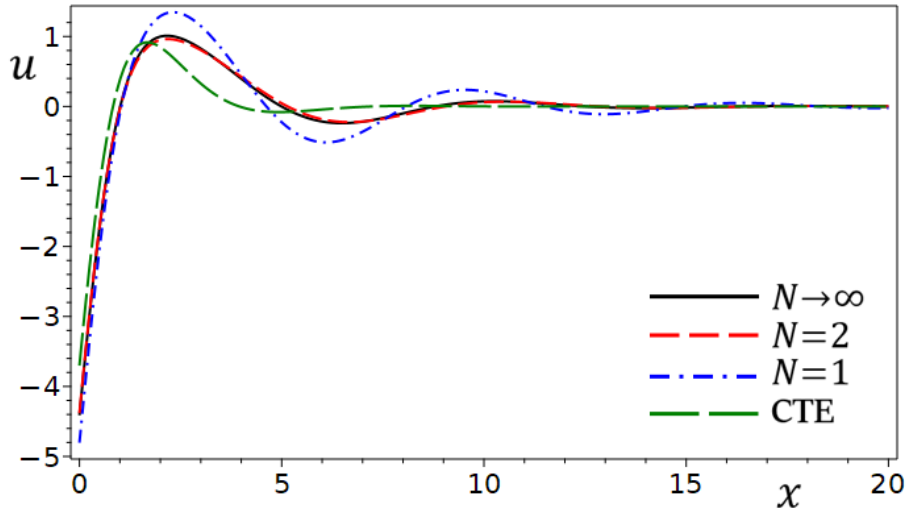

Figure 2: Variation of displacement distribution u with horizontal distance x for different N using CTE and LS theories.

imum peak value differs among models, with the $N = 1$ case giving the largest overshoot. For $N = 1$, the displacement curve exhibits stronger oscillations with higher amplitude, deviating more from CTE. For $N = 2$, the oscillations are weaker, and the curve lies closer to the limiting case. For $N \to \infty$, the displacement smooths out further, closely following the CTE prediction with mild oscillatory features. The CTE solution shows a smoother transition, with no oscillations beyond the peak. In contrast, the LS-based solutions capture wave-like behavior in the displacement due to the finite thermal relaxation time. At larger x, LS curves with higher N converge toward the CTE result. Long-distance behavior ($x > 10$), all curves tend toward zero displacement, with oscillations gradually vanishing. The simple LS results ($N = 1$) show damped oscillations, while CTE decays smoothly without oscillations.

Figure 3 displays the variation of displacement distribution v with horizontal distance x using CTE theory and LS thermoelasticity theory for different values of N. The classical thermoelasticity solution exhibits a smoother response with relatively small oscillations in the transverse displacement v. Its profile damps out quickly as x increases. The LS model with $N = 1$ predicts stronger oscillatory behavior, especially near the origin ($x < 5$), where the amplitude of v is significantly larger than that of the CTE and higher-order LS models. This designates that the lower-order truncation of the expansion enhances wave dispersion and amplifies oscillations. The LS model with $N = 2$ delivers a closer approximation to the $N \to \infty$ case, reducing the overshoot and oscillations observed in the $N = 1$ case. The refined LS model ($N \to \infty$) serves as the converged solution. Its distribution closely matches the $N = 2$ curve, confirming that a relatively low-order expansion is sufficient to capture the essential physics. Increasing N decreases the discrepancy between LS predictions and the limiting case ($N \to \infty$). The CTE model fails to capture these wave-like oscillations, highlighting the advantage of generalized thermoelasticity theories, similar to LS.

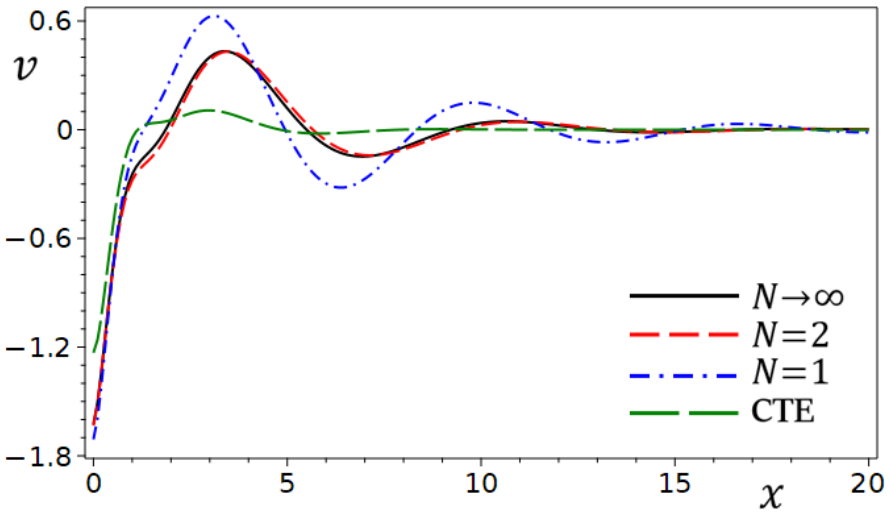

Figure 3: Variation of displacement distribution v with horizontal distance x for different N using CTE and LS theories.

Figure 4 illustrates the variation of dilatation distribution e with horizontal distance x for different N using CTE and LS theories. The dilatation e jumps from a large positive value near the surface ($x = 0$), reflecting the strong thermal expansion at the boundary. With increasing x, e decays rapidly, then oscillates about zero before finally tending to equilibrium ($e \to 0$). The CTE produces a smooth, monotonic decay from the initial peak. No oscillations appear, consistent with pure diffusion behavior. The LS theory with $N = 1$ shows pronounced oscillations around zero, with a strong undershoot below -1 near $x \approx 5$. This is the most dispersive response, indicating the presence of thermal wave effects. For LS with $N = 2$, oscillations are greatly reduced compared to $N = 1$. The profile tracks closer to the monotonic trend while retaining mild wave-like features. For LS with $N \to \infty$, the response nearly coincides with $N = 2$, indicating rapid convergence of the expansion. The oscillations are almost suppressed, giving a curve much closer to CTE, but with a slightly higher initial peak and smoother decay.

Figure 5 shows the variation of the normal stress distribution σ_{11} with horizontal distance x for different N using CTE and LS theories. The normal stress σ_{11} shows oscillatory variation with horizontal distance x, unlike a purely monotonic decay. Starting near zero at the boundary, the stress builds to a peak tensile value, then oscillates between positive (tensile) and negative (compressive) values before gradually damping toward zero at larger distances. The CTE theory exhibits a smooth, weakly oscillatory profile with a smaller amplitude. The stress amplitude remains low, showing a diffusion-like response without strong wave effects. The LS with $N = 1$ gives the largest oscillations with a sharp tensile peak (~ 2.5) around $x \approx 4$, followed by a strong compressive trough below -1. Additional oscillatory lobes appear at larger x. This highlights the wave-dominated nature of the single-term LS model. For LS with $N = 2$, oscillations are damped significantly, with stress values closely tracking the converged curve. The main tensile peak and subsequent compressive dip are smaller compared to $N = 1$, indicating enhanced stability. The

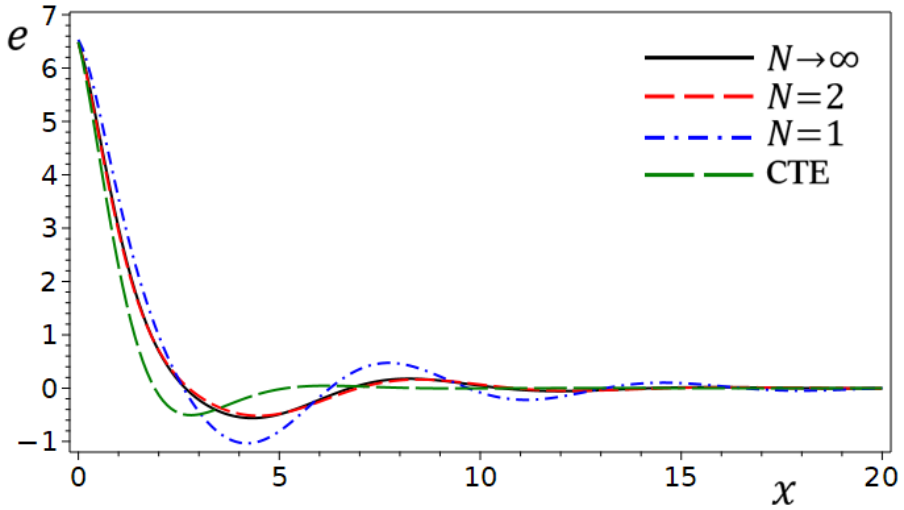

Figure 4: Variation of dilatation distribution e with horizontal distance x for different N using CTE and LS theories.

LS with $N \to \infty$ delivers a smooth, converged profile with oscillations strongly reduced compared to $N = 1$. The stress curve is nearly identical to the $N = 2$ result, confirming rapid convergence of the expansion.

Figure 6 illustrates the variation of the normal stress distribution σ_{22} with horizontal distance x for different N using CTE and LS theories. The stress component σ_{22} differs oscillatorily with horizontal distance x, showing both compressive and tensile regions. The response is stronger near the boundary, with oscillations gradually decaying toward zero as x increases. The CTE theory displays a smooth, weak oscillatory profile with relatively small amplitudes. The maximum tensile stress is lower than in the LS theory, and oscillations decay more quickly. Indicates purely diffusive stress propagation without strong wave effects. The simple LS theory ($N = 1$) shows the largest oscillations: A strong compressive trough at $x \approx 0$ reaching -3. Followed by a sharp tensile peak (~ 3) around $x \approx 4$. Additional oscillatory lobes at larger distances. This demonstrates that truncation at $N = 1$ leads to exaggerated wave amplitudes. For LS with $N = 2$, oscillations are much more stable, closely tracking the converged solution. The main compressive and tensile peaks are present but with reduced amplitudes compared to $N = 1$. The LS theory with $N \to \infty$ delivers the reference converged solution, showing a realistic stress-wave profile with controlled oscillations. Nearly identical to the $N = 2$ case, confirming fast convergence with increasing N.

Figure 7 shows the variation of the tangential stress distribution σ_{12} with horizontal distance x for different N using CTE and LS theories. The tangential stress displays a damped oscillatory profile with respect to horizontal distance x. Unlike the normal stresses (σ_{11}, σ_{22}), the amplitude of σ_{12} is much smaller (maximum around 0.5), reflecting the secondary nature of shear stresses compared to the dominant normal stresses under thermal loading. Oscillations diminish gradually as $x \to 20$, approaching zero. The CTE theory predicts relatively low shear stress levels, with a smooth and slowly decaying

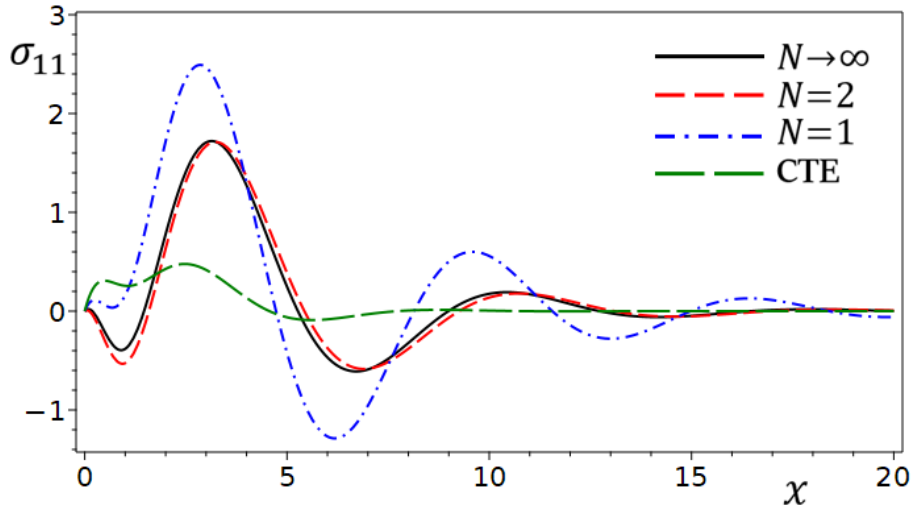

Figure 5: Variation of normal stress distribution σ_{11} with horizontal distance x for different N using CTE and LS theories.

response. Oscillations are weak compared to LS, showing diffusion-like stress transfer. The simple LS produces the largest oscillations with alternating peaks and troughs. The first tensile peak (≈ 0.45) occurs near $x \approx 1.5$, followed by a compressive trough at $x \approx 4.5$. Overestimates the shear response, similar to what was seen for σ_{11} and σ_{22}. For the LS theory with $N = 2$, shear stresses are much closer to the converged solution. Oscillations are well represented, but amplitudes are moderated compared to $N = 1$. The LS theory with $N \to \infty$ provides the stable reference solution, with realistic shear stress oscillations. Nearly identical to the $N = 2$ case, confirming rapid convergence of the truncated series expansion.

Figure 8 shows the 3D distribution of temperature θ using LS theory ($N \to \infty$) in (a) x-y plane and (b) space-time domain. In Fig. 8(a), the temperature θ is largest near the heated edge, reaching a pronounced positive peak. Moving away from the boundary, θ shows a peak–trough sequence (positive peak $\to$ negative undershoot $\to$ small ripples) that decays rapidly with x. This is the hallmark of the LS finite-speed heat conduction. Across $0 \leq y \leq 2$, the surface is nearly ridge-like—amplitude slightly decreases with y and the oscillations smooth out, indicating mild transverse attenuation (and a small phase lag) compared with the dominant transport along x. For larger x, the surface flattens toward $\theta \approx 0$, showing that the thermal disturbance is localized near the boundary and becomes negligible at a distance. So, in the exponential LS limit, heat propagates as damped thermal waves primarily along x, with only modest lateral (y) dispersion, yielding a smoothly decaying 3D temperature field.

In Fig. 8(b), at the surface $x = 0$, the temperature θ reaches its highest value, reflecting the imposed harmonic heating. As x increases, θ exhibits an oscillatory decay pattern—a strong positive peak followed by a negative trough and smaller ripples. This reflects finite-speed thermal wave propagation predicted by the LS model. For increasing t (from 0.3 to 0.7), the amplitude of oscillations decreases gradually, and the thermal field tends to

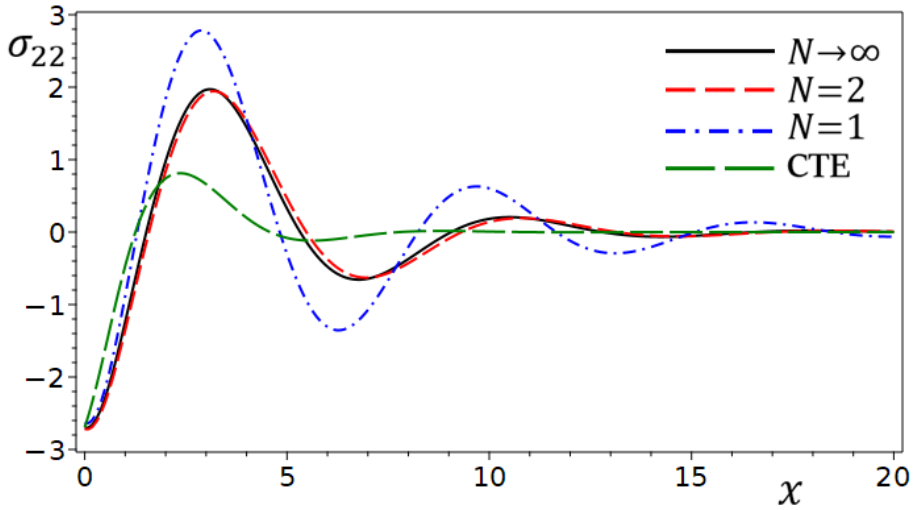

Figure 6: Variation of normal stress distribution σ_{22} with horizontal distance x for different N using CTE and LS theories.

flatten out, indicating temporal damping of the heat wave. The oscillations diminish more quickly with distance in x than with time in t, confirming that heat transport is strongly localized near the heated boundary. At larger x and later t, the surface approaches $\theta \approx 0$, meaning the disturbance vanishes and the medium relaxes toward equilibrium. So, under LS theory with $N \to \infty$, the temperature field in the space–time domain demonstrates damped thermal wave propagation that weakens with both distance and time, highlighting the finite propagation speed and non-Fourier behavior of the model.

Both plots in Fig. 8 show a large peak at the heated boundary ($x = 0$) and a damped oscillatory decay as x increases—signature of LS thermal waves (finite-speed, non-Fourier). The LS exponential limit yields a thermal field that propagates as a damped wave primarily in x. Across y the field is relatively uniform (mild lateral dispersion), whereas over time the same field loses amplitude and smooths out—capturing the finite-speed conduction with relaxation that distinguishes LS from classical diffusion.

Figure 9 shows the 3D distribution of displacement u using LS theory ($N \to \infty$) in (a) x-y plane and (b) space-time domain. The displacement in Fig. 9(b) displays its largest negative values at the boundary ($x = 0$), consistent with the strong thermoelastic response to localized heating. This suggests that thermal expansion near the surface causes significant compressive or inward motion. As x increases, the amplitude of uuu decays gradually, approaching a nearly uniform small value. This reflects the finite-speed propagation and relaxation characteristic of the LS model. The displacement surface shows weak but noticeable oscillatory behavior in the y-direction. The variations are smoother than along in x, indicating that lateral effects are less pronounced compared to depth-wise transport. Beyond a short distance into the medium, the displacement changes sign, showing alternating compressive and tensile zones. This wave-like oscillation is a hallmark of non-Fourier heat conduction coupled with elasticity.

In Fig. 9(b), at early times ($t \approx 0.3$), the displacement reaches its maximum ampli-

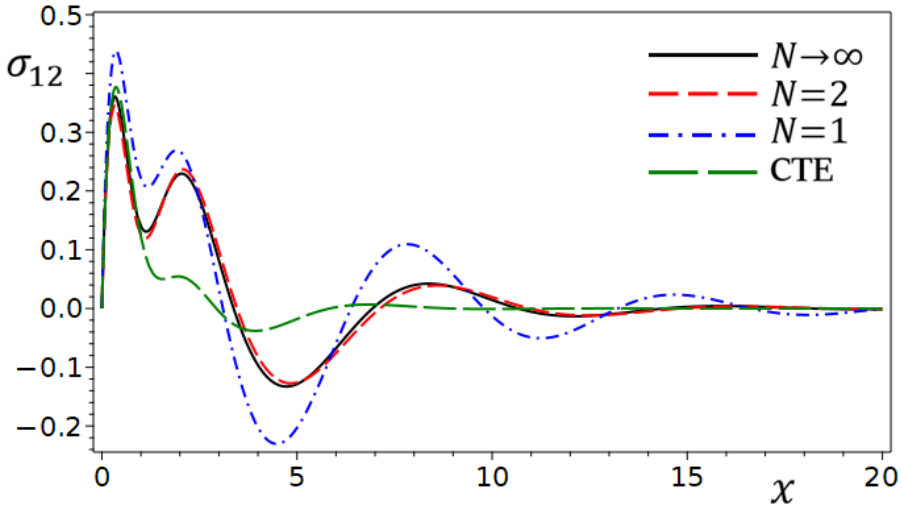

Figure 7: Variation of tangential stress distribution σ_{12} with horizontal distance x for different N using CTE and LS theories.

tude near the boundary, indicating the immediate thermoelastic response to the applied thermal load. As in Fig. 9(a), the amplitude of u diminishes with increasing x. This confirms the damped wave nature of displacement propagation predicted by LS theory. The displacement shows oscillatory changes with time at fixed x, starting with a sharp rise, then alternating between compressive and tensile states. The oscillations dampen as t increases, eventually approaching a quasi-steady state. The surface shows clear traveling-wave characteristics: the displacement disturbances move outward in x as t increases, rather than diffusing instantly as in classical thermoelasticity.

Figure 9 illustrates that under the exponential LS model, the thermal excitation at the boundary generates finite-speed, damped displacement waves: the largest inward/outward motions occur at the heated surface, propagate into the medium as oscillatory fronts, and attenuate with both distance and time, while lateral variations remain comparatively weak.

Figure 10 shows the transverse displacement v under the exponential LS model ($N \to \infty$). In Fig. 10(a), $v(x, y)$ at fixed t shows that the largest $|v|$ occurs at the heated surface $x = 0$; amplitude decays rapidly with depth. The lateral variation in y is present but much weaker than the x-dependence, producing gentle ripples superposed on the strong through-thickness decay. The displacement v changes sign, revealing an alternating shear-type response induced by the thermal loading. In Fig. 10(b), $v(x, t)$ in space-time shows that early times yield stronger oscillations and steeper gradients near $x = 0$; with increasing t, oscillations damp and the profile smooths. The disturbances propagate inward with finite speed (wavefronts) and attenuate in both x and t.

In Fig. 10, both plots confirm that v is generated at the boundary and decays quickly into the solid, consistent with a damped wave rather than a diffusive spread. The spatio-temporal surface in Fig. 10(b) makes the traveling nature of the disturbance explicit. While in Fig. 10(a), it captures its instantaneous spatial footprint. The variation across y is secondary; the dominant transport and coupling are along x (normal to the heated face).

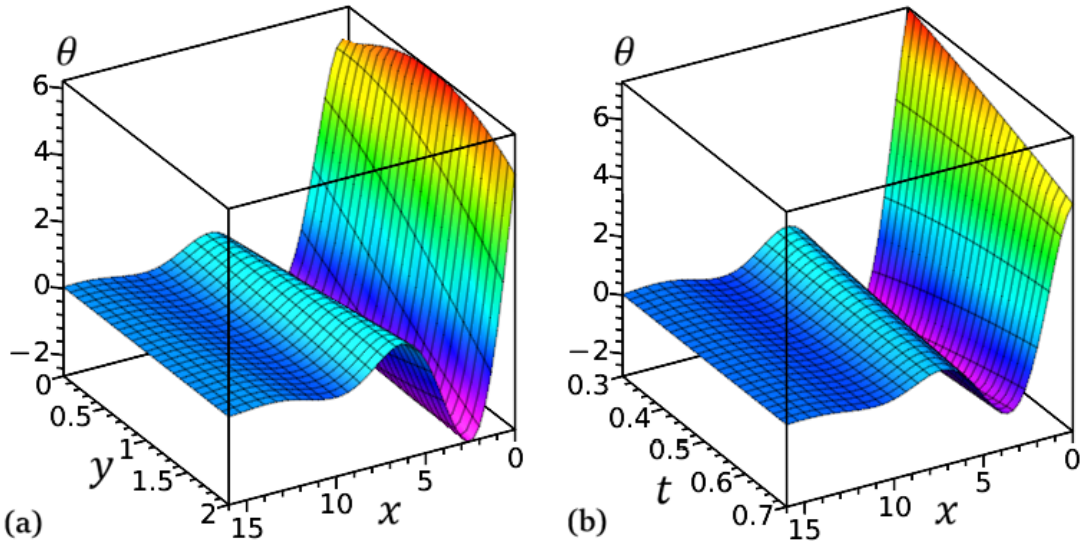

Figure 8: 3D distribution of temperature θ using LS theory ($N \to \infty$) in (a) x-y plane and (b) space-time domain.

The sign changes in v across x and t reflect alternating shear states as the thermoelastic wave passes.

Figure 11 shows the 3D distribution of dilatation e using LS theory ($N \to \infty$) in (a) x-y plane and (b) space-time domain. In Fig. 11(a), the dilatation e reaches its maximum at the boundary where the thermal load is applied. The values are significantly higher here, indicating strong volumetric expansion due to intense surface heating. As x increases (moving deeper into the medium), e decreases steeply, showing that volumetric expansion is strongly localized near the surface and diminishes quickly with depth. Small oscillations appear in e as x increases, suggesting wave-type propagation of the thermoelastic disturbance, characteristic of LS theory with finite thermal wave speed. The dilatation shows only mild dependence on the lateral direction y, remaining nearly uniform across it. The dominant gradient is along x.

In Fig. 11(b), the dilatation is maximum at the heated boundary, reaching values above 8 units, higher than the x-y profile in Fig. 11(a). This designates a very strong thermoelastic expansion localized at the surface. As x increases, e decreases rapidly, showing that the thermoelastic response weakens as the disturbance propagates inward. At early times ($t \approx 0.3$), dilatation is strongest near the boundary, showing the immediate response to thermal shock. As time increases ($t \to 0.7$), the dilatation decreases gradually, reflecting energy dissipation and attenuation of thermoelastic waves with time. The oscillatory/ripple patterns along x are preserved over time, but their amplitude diminishes. The distribution suggests finite-speed propagation of thermoelastic waves (a hallmark of LS theory), as opposed to purely diffusive behavior in classical Fourier models.

The dilatation under the LS model is a surface-initiated, finite-speed, damped volumetric wave: it peaks at $x = 0$, decays rapidly with depth, and relaxes with time—showing

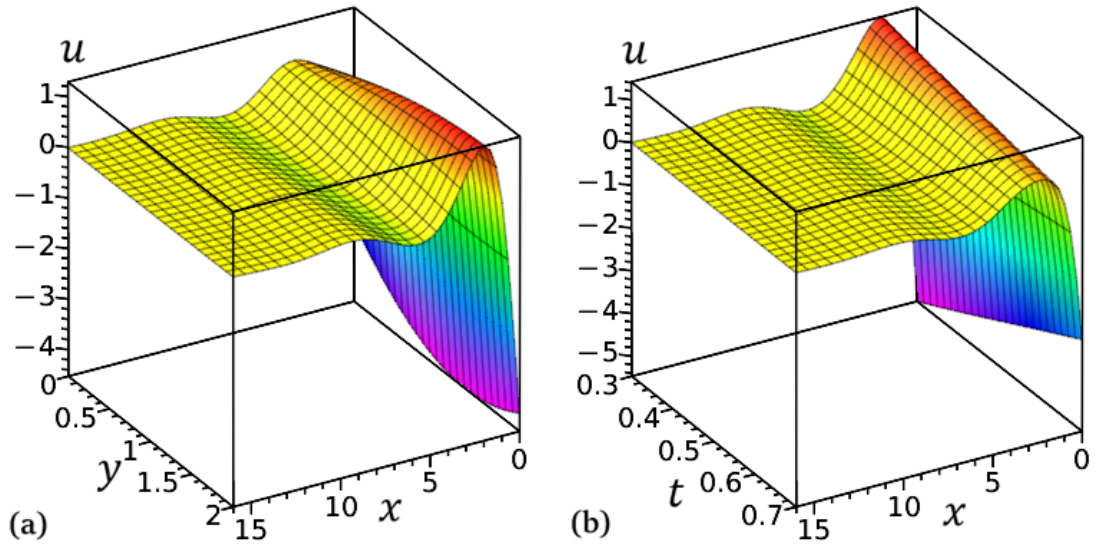

Figure 9: 3D distribution of displacement u using LS theory ($N \to \infty$) in (a) x-y plane and (b) space-time domain.

weak lateral variation and strong through-thickness, transient behavior.

Figure 12 shows the 3D distribution of normal stress σ_{11} using LS theory ($N \to \infty$) in (a) x-y plane and (b) space-time domain. In Fig. 12(a), the 3D distribution of the normal stress σ_{11} in the x-y plane under LS theory ($N \to \infty$) shows that the stress is surface-localized with pronounced oscillatory peaks near the boundary ($x = 0$). The stress amplitude decreases with depth (y), indicating that thermoelastic stresses are strongest at the heated surface and decay as the wave propagates inward. The oscillatory nature reflects the wave-like character of the LS model. In Fig. 12(b), the 3D distribution of σ_{11} in the x-t domain shows that it is highly time-dependent, with sharp peaks at early times that gradually attenuate as time progresses. The oscillatory behavior along x highlights the propagation of stress waves away from the surface, while the decay over time confirms the damping effects inherent to the LS theory.

The normal stress σ_{11} under LS theory ($N \to \infty$) is controlled by transient thermoelastic waves that originate at the heated boundary, showing strong surface localization, oscillatory wavefronts, and rapid attenuation with both depth and time. These results confirm the wave-propagation nature of the LS model, where stresses are not diffusive but instead travel as damped elastic waves.

Figure 13(a) displays the 3D distribution of normal stress σ_{22} using LS theory ($N \to \infty$) in the x-y plane. The stress magnitude is largest near the boundary surface ($x \approx 0$) and decays with increasing depth (x). The pattern alternates between compressive and tensile, indicating the propagation of thermoelastic stress waves. The stress variation with y is relatively smooth and less pronounced, highlighting that the dominant stress response occurs along the x-direction (depth) rather than across y. Regions of compression and tension coexist, consistent with thermoelastic wave reflections and superposition effects

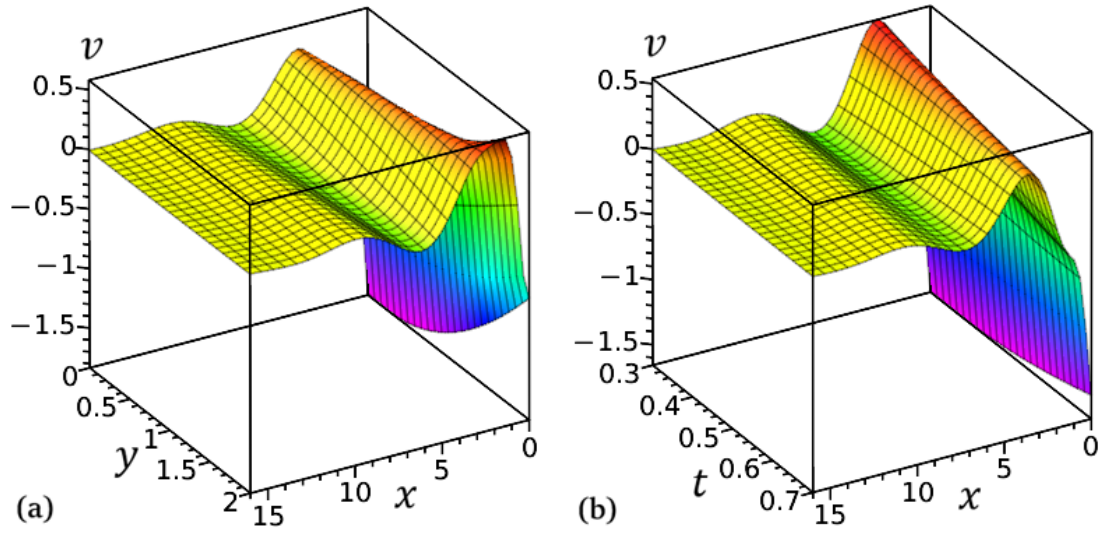

Figure 10: 3D distribution of displacement v using LS theory ($N \to \infty$) in (a) x-y plane and (b) space-time domain.

within the medium. So, the normal stress σ_{22} under the LS theory is strongly concentrated near the surface and propagates inward as damped thermoelastic waves with alternating tensile–compressive character, while variations across y remain limited compared to depth variations.

Figure 13(b) exhibits the 3D distribution of normal stress σ_{22} using the LS theory ($N \to \infty$) in the space-time domain. The stress exhibits strong peaks at very early times ($t \approx 0.3$), particularly near the surface ($x \approx 0$), showing the immediate thermoelastic response to the applied thermal loading. Similar to Fig. 13(a), the maximum stress is concentrated at the surface, gradually decaying with depth (x) as thermoelastic waves propagate inward. Oscillatory tensile–compressive stress patterns emerge, but their amplitude decreases over time, confirming the dissipative nature of the LS theory. As time advances, the stress σ_{22} diminishes significantly, reflecting both spatial and temporal damping of the thermoelastic disturbance. So, σ_{22} in the space-time domain is highly transient and surface-localized, with strong early-time stress peaks that decay rapidly in both space and time. This behavior illustrates the damped propagation of thermoelastic normal stress waves under LS theory.

Finally, Figure 14 shows the 3D distribution of the tangential stress σ_{12} using LS theory ($N \to \infty$) in (a) x-y plane and (b) space-time domain. In Fig. 14(a), σ_{12} rises sharply at lower values of x (near the origin), reaching its peak in the region $x \approx 2$ to 5, while further along the x-axis the stress amplitude decreases and oscillates with a diminishing trend. Along the y-axis, the stress shows a rapid decay as y increases, indicating that tangential stresses are more concentrated near the surface region (low y) and gradually dissipate into the depth of the medium.

The plot in Fig. 14(b) presents the tangential stress σ_{12} as a function of space (x)

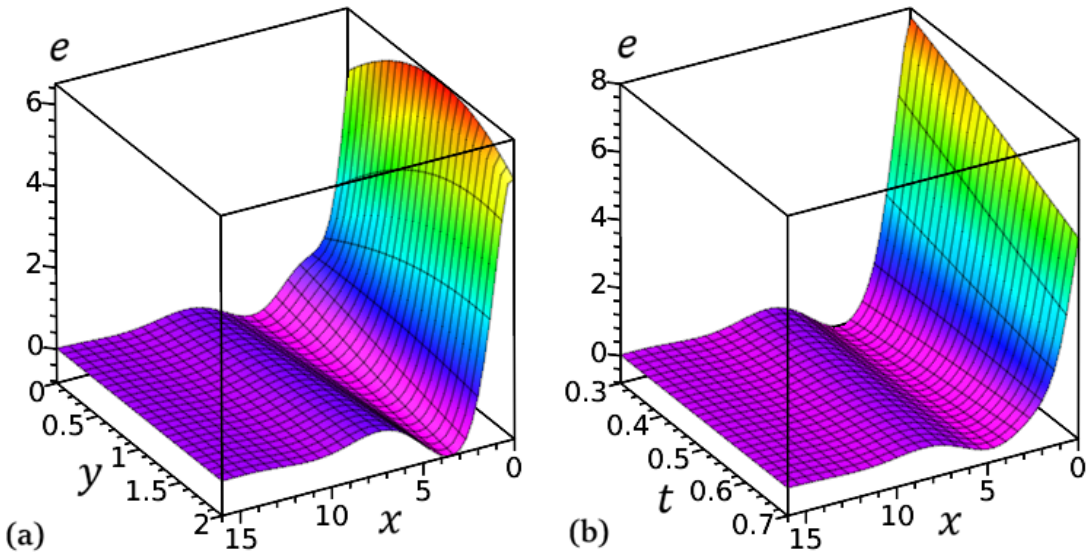

Figure 11: 3D distribution of dilatation e using LS theory ($N \to \infty$) in (a) x-y plane and (b) space-time domain.

and time (t). The stress is initially large at small times, especially close to the boundary region (low x), showing a sharp rise that forms a stress front. As time progresses, the stress profile spreads in the x-direction, with oscillatory attenuation, meaning that stress waves propagate and weaken with both distance and time. Negative stress values perform in certain regions, representing stress reversal (phase lag effect), consistent with relaxation processes in the LS thermoelastic theory.

In general, Fig. 14 highlights that under the LS generalized thermoelasticity framework ($N \to \infty$), the tangential stress σ_{12} exhibits localized peaks near the boundary and decays with both depth (y) and time (t). The oscillatory nature of the distributions confirms the wave-like propagation of thermoelastic stresses with finite speed (a key feature of LS theory), combined with relaxation damping. This demonstrates that shear stresses are most significant near the loaded boundary and at early times, but they diminish progressively in both space and time due to thermoelastic diffusion and wave attenuation.

6. Conclusions

In this study, the exponential LS model predicts finite-speed, damped thermoelastic waves originating at the heated surface. The response is surface-localized and decays rapidly with x; lateral spread is small. Temporal evolution shows initial strong response $\to$ oscillatory relaxation $\to$ decay to equilibrium. Classical thermoelasticity (CTE), which would expect smoother, non-wave diffusive displacement without travelling fronts, is qualitatively different from this behaviour. The thermal wave propagation predicted by LS theory is strongly influenced by the operator expansion order N. Stronger thermal wave effects are reflected in the more noticeable oscillations caused by the truncation at low N.

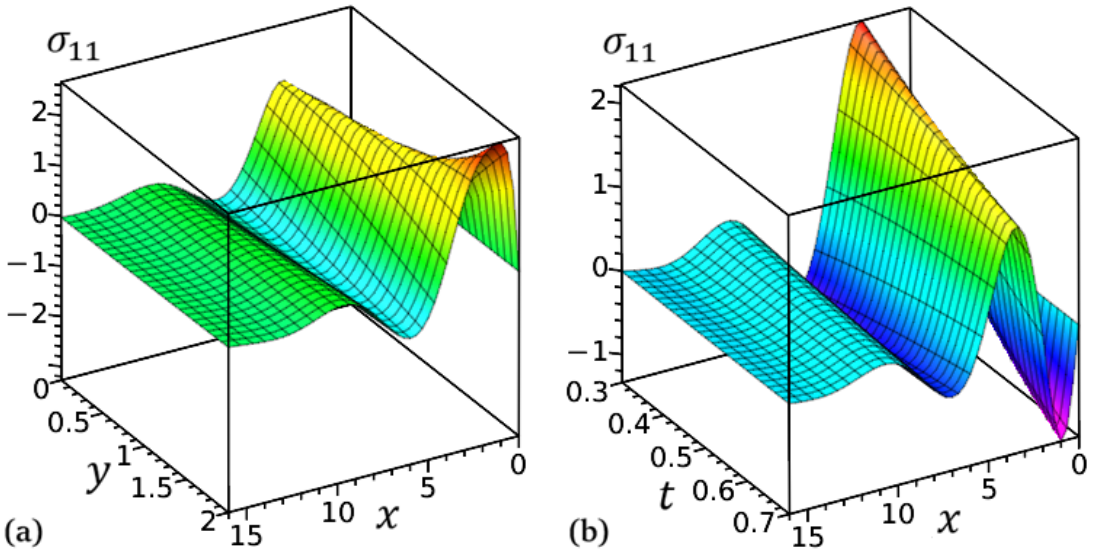

Figure 12: 3D distribution of normal stress σ_{11} using LS theory ($N \to \infty$) in (a) x-y plane and (b) space-time domain.

Higher N makes the solution smoother and more in line with the CTE results and the limiting situation. Unlike the LS theory, the CTE theory is unable to capture oscillatory wave-like properties because it lacks a relaxing effect.

Damped thermoelastic waves are superimposed over the diffusive response by thermal relaxation (LS), and dispersion and overshoot are controlled by the truncation order N. Higher N produces quick convergence towards the infinite-order (exponential) LS limit and systematically reduces spurious oscillations. The transverse displacement v is more dispersive than the longitudinal u at low N, so adopting $N \geq 2$ (or the exponential form $N \to \infty$) is advisable for accurate, physically smooth predictions of both components.

The dilatation is highly sensitive to the truncation order N. The simple LS case ($N = 1$) exaggerates oscillations, while $N = 2$ and especially $N \to \infty$ provide refined, smooth responses that closely approximate the CTE trend but still retain thermal relaxation effects. The normal stress distribution illustrates the wave-dominated response of LS thermoelasticity compared to the diffusion-dominated behavior of classical thermoelasticity. While truncation at $N = 1$ exaggerates oscillations, higher-order truncations ($N = 2$ or $N \to \infty$) provide accurate, stable stress fields. This confirms that the exponential LS model converges quickly and reliably captures thermal-stress wave propagation effects.

The tangential stress follows a wave-like but less intense distribution compared to the normal stresses. The LS theory captures shear stress oscillations realistically, while the CTE model underestimates them. The convergence with $N = 1$ is rapid, with $N = 2$ already approximating the infinite case very closely. For stress prediction under thermoelastic waves, use LS with at least $N = 2$ (or the $N \to \infty$ exponential form) to obtain stable, physically credible stress fields. Normal stresses carry the primary thermoelastic wave signature; shear stress is secondary and smaller in magnitude. The exponential LS

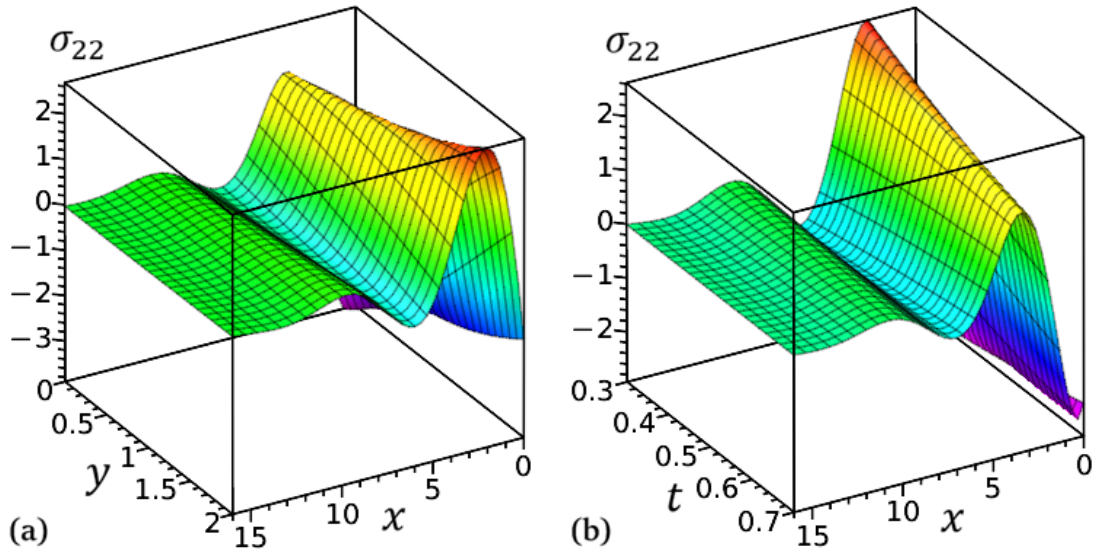

Figure 13: 3D distribution of normal stress σ_{22} using LS theory ($N \to \infty$) in (a) x-y plane and (b) space-time domain.

limit offers a clean, damped wave response that reconciles wave effects with numerical stability—something the classical theory and the $N = 1$ truncation each miss in different ways.

According to LS thermoelasticity theory, the displacement u exhibits weaker lateral variation, propagates as damped oscillations into the medium, and is strongly localised close to the heated border. In contrast to the strictly diffusive trend predicted by conventional thermoelasticity, the results demonstrate the finite-speed, wave-like behaviour of thermoelastic reactions. The transverse displacement v under the exponential LS model is a secondary, shear-dominated, finite-speed response; it is strongest at the heated boundary, propagates inward as a damped thermoelastic wave, exhibits mild lateral variation, and relaxes toward equilibrium as time advances. The dilatation under the exponential LS model is substantially surface-localized, declining quickly with depth and showing sharp peaks close to the heated boundary. Strong initial responses that rapidly diminish in both space and time characterise its extremely time-dependent evolution. The deformation is dominated by normal expansion along the boundary surface, reflecting the brief, wave-like propagation of thermoelastic volumetric strain.

The results show that the displacement, dilatation, and normal stress fields are significantly concentrated around the heated surface and rapidly diminish with depth. The displacement exhibits damped oscillations, but the dilatation highlights the primary surface-driven volumetric expansion. The stress distribution, which alternates between tension and compression, illustrates the passage of thermoelastic waves. All fields display significant peaks at early times that progressively fade in the space-time domain, as predicted by LS theory, illustrating the transitory and wave-like nature of thermoelastic response. Under LS theory with an exponential ($N \to \infty$) operator, σ_{22} is a transient, surface-

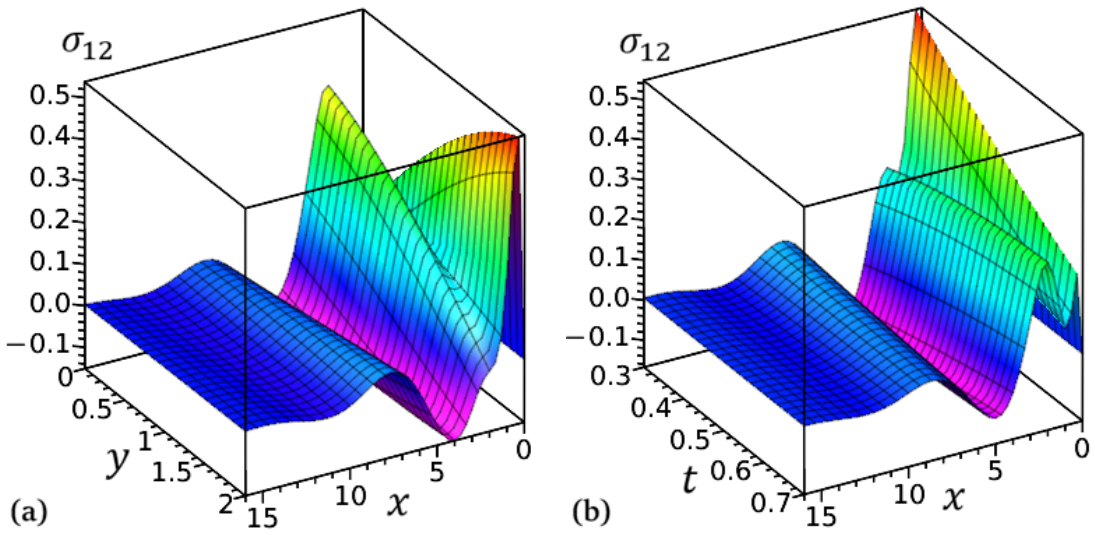

Figure 14: 3D distribution of tangential stress σ_{12} using LS theory ($N \to \infty$) in (a) x-y plane and (b) space-time domain.

localized normal stress that propagates inward as a damped thermoelastic wave. Peak loads occur close to the boundary and shortly after heating begins, then attenuate quickly in both space and time—an important design cue for predicting where and when maximum stresses will arise.

Tangential stresses are concentrated in the near-surface region, as confirmed by the tangential stress σ_{12} in the spatial domain, which shows prominent peaks close to the boundary and rapidly decreases with depth. In the space-time domain, σ_{12} exhibits a strong rise at first, then oscillatory attenuation, which suggests that stress waves are propagating at a finite speed before relaxing. Overall, the findings show that the transient wave-like behaviour and localised nature of thermoelastic shear stresses, which decrease with increasing time and distance, are both captured by the LS theory.

Data availability

Data available on request from the authors. The data that support the findings of this study are available from the corresponding author upon reasonable request.

Declarations

Conflict of interest: The authors declare that there is no conflict of interest.

Ethical approval: This article does not contain any studies with human participants or animals performed by any of the authors.

Funding

Author with funding: Zahra S. Hafed
Funder name: King Khalid University
Grant ID: RGP2/115/46

Acknowledgements

The authors extend their appreciation to the Deanship of Research and Graduate Studies at King Khalid University for funding this work through the Large Research Project under grant number RGP2/115/46.

Author Contributions

- Conceptualization: Z.S. Hafed, A.M. Zenkour
- Methodology: Z.S. Hafed, A.M. Zenkour
- Software: Z.S. Hafed
- Validation: A.M. Zenkour
- Formal analysis: Z.S. Hafed
- Investigation: Z.S. Hafed, A.M. Zenkour
- Writing—original draft preparation: Z.S. Hafed, A.M. Zenkour
- Writing—review and editing: A.M. Zenkour
- Visualization: Z.S. Hafed, A.M. Zenkour

References

[1] H.W. Lord and Y.A. Shulman. A generalized dynamical theory of thermoelasticity. *J. Mech. Phys. Solids*, 15:299–309, 1967.
[2] H.H. Sherief and M.N. Anwar. A problem in generalized thermoelasticity for an infinitely long annular cylinder. *Int. J. Engng Sci.*, 26(3):301–306, 1988.
[3] M.I.A. Othman. Lord–shulman theory under the dependence of the modulus of elasticity on the reference temperature in two-dimensional generalized thermoelasticity. *J. Therm. Stresses*, 25:1027–1045, 2002.
[4] M.I.A. Othman. Effect of rotation and relaxation time on a thermal shock problem for a half-space in generalized thermo-viscoelasticity. *Acta Mech.*, 174:129–143, 2005.
[5] R. Kumar and L. Rani. Deformation due to mechanical and thermal sources in generalized thermoelastic half-space with voids. *J. Therm. Stresses*, 28:123–145, 2005.

[6] H.M. Youssef. Two-dimensional generalized thermoelasticity problem for a half-space subjected to ramp-type heating. *Europ. J. Mech. A/Solids*, 25:745–763, 2006.
[7] N.M. El-Maghraby. A two-dimensional generalized thermoelasticity problem for a half-space under the action of a body force. *J. Therm. Stresses*, 31:557–568, 2008.
[8] I.A. Abbas, A.N. Abd-alla, and M.I.A. Othman. Generalized magneto-thermoelasticity in a fiber-reinforced anisotropic half-space. *Int. J. Thermophys*, 32:1071–1085, 2011.
[9] H.H. Sherief, M.N. Allam, and M.A. El-Hagary. Generalized theory of thermoviscoelasticity and a half-space problem. *Int. J. Thermophys*, 32:1271–1295, 2011.
[10] H.H. Sherief and A.M. Abd El-Latief. Application of fractional order theory of thermoelasticity to a 1d problem for a half-space. *ZAMM, Z. Angew. Math. Mech.*, 94(6):509–515, 2014.
[11] Y. Kiani and M.R. Eslami. Nonlinear generalized thermoelasticity of an isotropic layer based on lord-shulman theory. *Europ. J. Mech. A/Solids*, 61:245–253, 2017.
[12] L. Rani. Disturbances in a generalized thermoelastic half-space with voids and microtemperatures due to a mechanical force. *J. Eng. Phys. Thermophys.*, 96(4):1103–1116, 2023.
[13] B. Singh, A. Kumar, and J. Singh. Reflection of generalized thermoelastic waves from a solid half-space under hydrostatic initial stress. *Appl. Math. Comput.*, 177:170–177, 2006.
[14] M.I.A. Othman and B. Singh. The effect of rotation on generalized micropolar thermoelasticity for a half-space under five theories. *Int. J. Solids Struct.*, 44(9):2748–2762, 2007.
[15] S. Kaushal, R. Kumar, and A. Miglania. Response of frequency domain in generalized thermoelasticity with two temperatures. *J. Eng. Phys. Thermophys.*, 83(5):1080–1088, 2010.
[16] B. Singh. Propagation of rayleigh wave in a two-temperature generalized thermoelastic solid half-space. *ISRN Geophysics*, 2013:1–6, 2013.
[17] M.I.A. Othman and Y.Q. Song. Effect of the thermal relaxation and magnetic field on generalized micropolar thermoelasticity. *J. Appl. Mech. Tech. Phys.*, 57(1):108–116, 2016.
[18] B. Singh and B. Singh. Reflection from free surface of a rotating generalized thermopiezoelectric solid half space. *J. Solid Mech.*, 10(1):57–66, 2018.
[19] H.H. Sherief, F.A. Hamza, and A.M. Abd El-Latief. Wave propagation study for axisymmetric 2d problems of a generalized thermo-visco-elastic half space. *J. Therm. Stresses*, 42(7):835–848, 2019.
[20] Kh. Lotfy, A.A. El-bary, M. Allan, and M.H. Ahmed. Generalized thermal microstretch elastic solid with harmonic wave for mode-i crack problem. *Arch. Thermodynam.*, 41(2):147–168, 2020.
[21] R. Tiwari. Magneto-thermoelastic interactions in generalized thermoelastic half-space for varying thermal and electrical conductivity. *Waves Random Complex Media*, 34(3):1795–1811, 2024.
[22] H. Tianhu, S. Yapeng, and T. Xiaogeng. A two-dimensional generalized thermal

shock problem for a half-space in electromagneto-thermoelasticity. *Int. J. Eng. Sci.*, 42(8/9):809–824, 2004.

[23] H.M. Youssef and A.A. El-Bary. Mathematical model for thermal shock problem of a generalized thermoelastic layered composite material with variable thermal conductivity. *CMST*, 12(2):165–171, 2006.

[24] P. Ram, N. Sharma, and R. Kumar. Thermomechanical response of generalized thermoelastic diffusion with one relaxation time due to time harmonic sources. *Int. J. Therm. Sci.*, 47(3):315–323, 2008.

[25] N.M. El-Maghraby and A.A. Abdel-Halim. A generalized thermoelasticity problem for a half space with heat sources under axisymmetric distributions. *Aust. J. Basic Appl. Sci.*, 4(8):3803–3814, 2010.

[26] N.M. El-Maghraby. A generalized thermoelasticity problem for a half-space with heat sources and body forces. *Int. J. Thermophys*, 31:648–662, 2010.

[27] S. Goswami and N. Sarkar. Wave propagation in thermoelastic media with relaxation time. *Math. Mech. Solids*, 2025.

[28] Z.S. Hafed and A.M. Zenkour. Thermal shock of anisotropic hollow cylinders via one relaxation time-fractional model. *Acta Mech.*, 2026.

[29] Z.S. Hafed and A.M. Zenkour. Thermal shock of a two-layer solid based on the refined lord–shulman model. *Mech. Advanc. Mater. Struct.*, 2026.

[30] H.M. Youssef and E.A. Al-Lehaibi. State-space approach of two-temperature generalized thermoelasticity of one-dimensional problem. *Int. J. Solids Struct.*, 44:1550–1562, 2007.

[31] M.A. Ezzat and H.M. Youssef. Three-dimensional thermal shock problem of generalized thermoelastic half-space. *Appl. Math. Model.*, 34:3608–3622, 2010.

[32] J.J. Tripathi, G.D. Kedar, and K.C. Deshmukh. Two-dimensional generalized thermoelastic diffusion in a half-space under axisymmetric distributions. *Acta Mech.*, 226:3263–3274, 2015.

[33] H.M. Youssef and E.A.N. Al-Lehaibi. The boundary value problem of a three-dimensional generalized thermoelastic half-space subjected to moving rectangular heat source. *Boundary Value Problems*, 2019:1–15, 2019.

[34] Y. Guo, H. Zhu, and C. Xiong. A two-dimensional generalized thermo-hydro-mechanical-coupled problem for a poroelastic half-space. *Waves Random Complex Media*, 30(4):738–758, 2020.

[35] S.M. Said. 2d problem of nonlocal rotating thermoelastic half-space with memory-dependent derivative. *Multidiscipline Model. Mater. Struct.*, 18(2):339–350, 2022.

[36] F. Alshaikh. Effects of thermal relaxation times and porosity in a lord-shulman and refined multi-phase lags model of generalized thermoelasticity. *Mech. Based Design Struct. Mach.*, 51(1):438–449, 2023.

[37] I. Sarkar and G. Singh. Thermodynamically consistent modified lord-shulman generalized thermoelasticity with strain-rate. *J. Appl. Mech.*, 90(3):1–8, 2023.

[38] A.M. Zenkour and M.H. Aljadani. Nonlocal harmonically varying heat in a magnetothermoelastic thick plate using simple and refined lord and shulman theories. *Mathematics*, 13(7):1160, 2025.

[39] H.A. Saleh. Problem in generalized thermoelasticity for a half-space under the action of a body force. *J. Therm. Stresses*, 28:253–266, 2005.

[40] M. Sobhy and A.M. Zenkour. Refined lord–shulman theory for 1d response of skin tissue under ramp-type heat. *Materials*, 15(18):6292, 2022.

[41] A.M. Zenkour, T. Saeed, and A.A. Al-Raezah. A 1d thermoelastic response of skin tissue due to ramp-type heating via a fractional-order lord–shulman model. *J. Comput. Appl. Mech.*, 54(3):365–377, 2023.

[42] M.H. Aljadani and A.M. Zenkour. Effect of magnetic field on a thermoviscoelastic body via a refined two-temperature lord–shulman model. *Case Studies Therm. Eng.*, 49:103197, 2023.

[43] A.A. Alghamdi and A.M. Zenkour. Refined one relaxation time-fractional theory for the thermoelastic response of circular cylinders with variable thermal conductivity. *Mathematics*, 13(21):3497, 2025.